MMT HYPERVELOCITY STAR SURVEY. II. FIVE NEW UNBOUND STARS

Warren R. Brown, Margaret J. Geller, and Scott J. Kenyon
Smithsonian Astrophysical Observatory, 60 Garden Street, Cambridge, MA 02138, USA;
wbrown@cfa.harvard.edu, mgeller@cfa.harvard.edu, skenyon@cfa.harvard.edu

ABSTRACT

We present the discovery of five new unbound hypervelocity stars (HVSs) in the outer Milky Way halo. Using a conservative estimate of Galactic escape velocity, our targeted spectroscopic survey has now identified 16 unbound HVSs as well as a comparable number of HVSs ejected on bound trajectories. A Galactic center origin for the HVSs is supported by their unbound velocities, the observed number of unbound stars, their stellar nature, their ejection time distribution, and their Galactic latitude and longitude distribution. Other proposed origins for the unbound HVSs, such as runaway ejections from the disk or dwarf galaxy tidal debris, cannot be reconciled with the observations. An intriguing result is the spatial anisotropy of HVSs on the sky, which possibly reflects an anisotropic potential in the central 10–100 pc region of the Galaxy. Further progress requires measurement of the spatial distribution of HVSs over the southern sky. Our survey also identifies seven B supergiants associated with known star-forming galaxies; the absence of B supergiants elsewhere in the survey implies there are no new star-forming galaxies in our survey footprint to a depth of 1–2 Mpc.

Key words: galaxies: individual (M31, Sextans B) – Galaxy: center – Galaxy: halo – Galaxy: kinematics and dynamics – stars: early-type

Online-only material: color figures, machine-readable table

1. INTRODUCTION

Unbound radial velocities distinguish hypervelocity stars (HVSs) from other main-sequence stars in the Galaxy. In Brown et al. (2005) we reported the first HVS: a short-lived $3\,M_\odot$ star traveling with a Galactic rest-frame velocity of $700 \pm 12\ \mathrm{km\,s^{-1}}$, twice the Milky Way's escape velocity at the star's distance of $\simeq 100$ kpc. The observed motion of the star is comparable to the escape velocity from the surface of the star and is thus difficult to explain with stellar dynamics. The maximum ejection velocity from stellar binary disruption mechanisms (Blaauw 1961; Poveda et al. 1967) is limited to $\sim 300\ \mathrm{km\,s^{-1}}$ for $3\,M_\odot$ stars (Leonard & Duncan 1988, 1990; Leonard 1991, 1993; Tauris & Takens 1998; Portegies Zwart 2000; Davies et al. 2002; Gualandris et al. 2005).

There is overwhelming evidence for a $4 \times 10^6\,M_\odot$ massive black hole (MBH) in the Galactic center (Ghez et al. 2008; Gillessen et al. 2009b). The MBH sits in a vast crowd of stars, including short-lived B stars with orbital periods as short as 15 years (Gillessen et al. 2009a) and pericenter velocities as high as 12,000 km s^{-1} (=4% of the speed of light; Ghez et al. 2005). Three-body interactions between stars and the MBH are inevitable in this environment and will naturally result in the ejection of unbound "HVSs" (Hills 1988). This ejection process also works for a binary MBH (Yu & Tremaine 2003).

A MBH in the Galactic center must produce HVSs, and known HVSs fit the MBH ejection picture. The observed unbound velocities, stellar nature, ejection time distribution, and Galactic latitude and longitude distribution of HVSs all support a Galactic center origin. Known HVSs have the spectral types of B stars, the same spectral type as the stars observed orbiting the central MBH. In all cases where photometric variability (Fuentes et al. 2006) or echelle spectroscopy (Przybilla et al. 2008b, 2008c; López-Morales & Bonanos 2008) is available, HVSs are confirmed to be short-lived main-sequence B stars. Even the observed number of HVSs is consistent with the

theoretically predicted MBH ejection rate (Yu & Tremaine 2003; Perets et al. 2007) and with the number of "S-stars" presently orbiting the MBH (Perets 2009a; Bromley et al. 2012). In the Hills three-body exchange scenario, S-stars are the former companions of HVSs (Ginsburg & Loeb 2006), a picture which may (Perets et al. 2009a) or may not (Madigan et al. 2011) be supported by the S-stars' eccentricity distribution. Proper motion measurements promise to more directly test the link between HVSs and the MBH in the Galactic center (e.g., Brown et al. 2010b).

Here, we present the results of our ongoing spectroscopic survey on the 6.5 m MMT telescope to find new HVSs. Our effective survey strategy is to target stars with the colors of $\simeq 3\,M_\odot$ stars—stars bluer than halo blue horizontal branch (BHB) stars but redder than foreground white dwarfs—that should not exist at faint magnitudes unless they were ejected into the outer halo as HVSs. In previous papers, we reported the discovery of 14 unbound HVSs and a comparable population of possibly bound HVSs over a fifth of the sky (Brown et al. 2006a, 2006b, 2007b, 2007c, 2009a, 2009b). Here we report five new unbound HVSs; the distribution of HVS angular positions on the sky is significantly anisotropic.

In Section 2, we describe our HVS Survey strategy and spectroscopic observations. In Section 3, we discuss the distribution of stars in the survey, and identify the bound and unbound HVSs. In Section 4, we discuss the HVSs, and in Section 5 we discuss their spatial anisotropy. We conclude in Section 6.

2. DATA

2.1. Target Selection Strategy

We select HVS candidates with the magnitudes and colors of 2.5–$4\,M_\odot$ stars in the outer halo; 2.5–$4\,M_\odot$ stars are luminous and allow us to explore a large volume of space. Selecting these stars maximizes our contrast with respect to the Milky Way's stellar population, because 2.5–$4\,M_\odot$ stars are bluer than halo
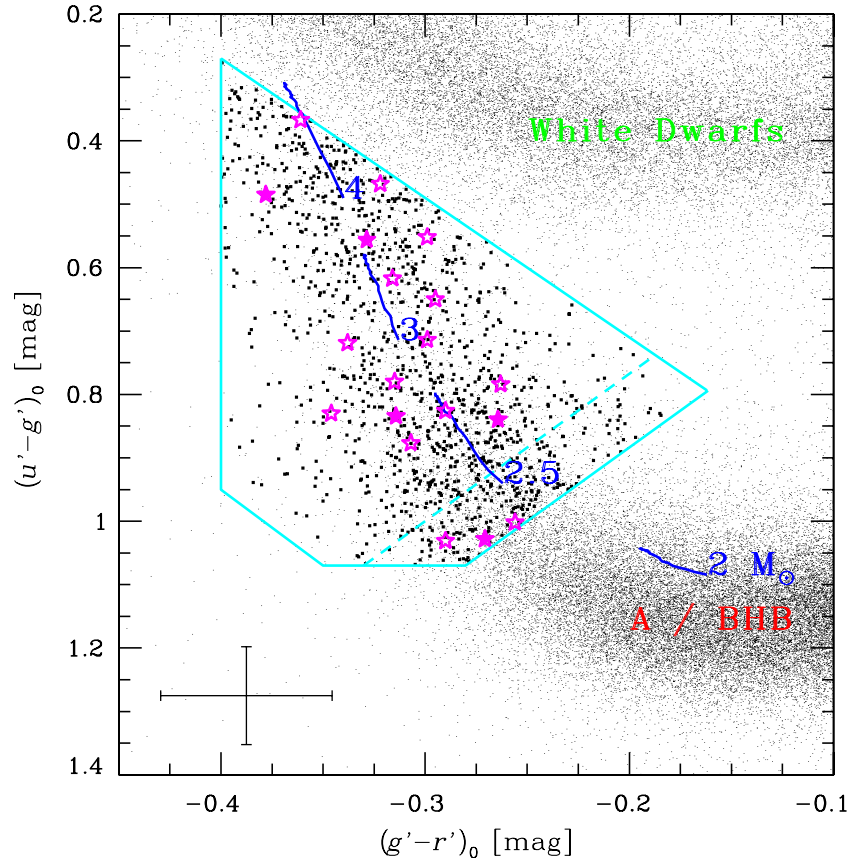
Figure 1. Color–color diagram showing the target selection for the unified HVS Survey (solid cyan line) and the observed candidates (black squares). The survey samples $17 < g < 20.25$ to the left of the dashed line and $19 < g < 20.25$ to the right of the dashed line as described in the text. Five new HVSs (solid magenta stars) and the fourteen previous HVSs (open magenta stars) scatter around the Girardi et al. (2004) stellar evolution tracks for 2.5–4 $M_\odot$ main-sequence stars (solid blue lines); numbers along the tracks indicate stellar mass. Average SDSS photometric uncertainties for a $g_0 = 19.5$ star are indicated by the error bars on the lower left. For reference, we plot the underlying distribution of stars in SDSS (black dots) and label the locus of white dwarfs and A-type/stars.

(A color version of this figure is available in the online journal.)

BHB stars and redder than disk white dwarfs. Targeting faint stars maximizes our efficiency for detecting HVSs because the density of normal Milky Way stars is very low in the outer halo. Finally, 2.5–4 $M_\odot$ stars have main-sequence lifetimes of a few $\times 10^8$ yr and thus should not exist at large distances unless they were ejected there.

We select candidates based on de-reddened point-spread function photometry from the Sloan Digital Sky Survey (SDSS; Aihara et al. 2011). Each SDSS data release (DR) changes its photometric calibration, however, which means that each DR contains candidates unique to that DR plus candidates in common with other DRs. Because we observe candidates taken from each subsequent DR, our HVS Survey is a concatenation of candidates selected from SDSS DR6, DR7, and DR8.

We begin with a cut on reddening $E(B-V) < 0.1$ to ensure accurate colors. We exclude the small region of the SDSS between $b < -l/5 + 50°$ and $b > l/5 - 50°$ to avoid excessive contamination from Galactic bulge stars. We also impose $-0.5 < (r-i)_0 < 0$ to eliminate non-stellar objects such as quasars.

Figure 1 illustrates our color selection. This color selection unifies the original HVS Survey that targets brighter and bluer objects (Brown et al. 2006a, 2006b, 2007b, 2007c) and our more recent HVS Survey that targets fainter and redder objects (Brown et al. 2009a). For reference, we plot in Figure 1 the underlying distribution of stars in SDSS and main-sequence tracks for 2 $M_\odot$, 2.5 $M_\odot$, 3 $M_\odot$, and 4 $M_\odot$ solar metallicity stars

(Girardi et al. 2002, 2004). Our color selection region targets the sequence of 2.5–4 $M_\odot$ stars bounded by $-0.4 < (g-r)_0 < (-0.43(u-g)_0 + 0.18)$ and $(2.2(g-r)_0 + 1.1) < (u-g)_0 < 1.07$.

Our magnitude selection is $17 < g_0 < 20.25$ in the region $(g-r)_0 < (-0.43(u-g)_0 + 0.13)$. In the region $(g-r)_0 > (-0.43(u-g)_0 + 0.13)$ we restrict ourselves to fainter magnitudes $18.6 + 10[(g-r)_0 + 0.3] + [(u-g)_0 - (1.2(g-r)_0 + 1.25)] < g_0 < 20.25$, or approximately $19 < g_0 < 20.25$.

Applying these selection criteria to the SDSS DR6, DR7, and DR8 photometric catalogs results in 874, 1097, and 1424 candidates, respectively. After removing objects such as nearby galaxies and bright stars by visual inspection, 1509 unique candidates remain. We previously published spectroscopic identifications and radial velocities for 609 of these candidates (plus a few hundred others that fall outside the present selection criteria) summarized in Brown et al. (2010b). SDSS provides spectroscopy for another 63 candidates. Thus there remain 837 candidates to be observed; we report observations of 497 of these candidates here.

2.2. Spectroscopic Observations

We obtained spectroscopy for 497 candidates at the 6.5 m MMT telescope during observing runs spanning 2008 December to 2011 October. All observations were obtained with the Blue Channel spectrograph (Schmidt et al. 1989) using the 832 line mm^{-1} grating in second order and either a 1″ or 1″.25

slit. These settings provide wavelength coverage 3600–4500 Å and a spectral resolution of 1–1.2 Å. All observations were obtained at the parallactic angle and were paired with comparison lamp exposures.

Our goal was to obtain modest signal-to-noise (S/N) observations adequate for determining radial velocity. At $g = 19$ mag we typically used a 390 s exposure to obtain $(S/N) \simeq 7$ pixel^{-1} in the continuum. We processed the spectra in real time to allow additional observations of interesting candidates. We extracted the spectra using IRAF[1] in the standard way and measured radial velocities using the cross-correlation package RVSAO (Kurtz & Mink 1998). The average statistical uncertainty of the radial velocity measurements is ± 11 km s^{-1}.

While we made an effort not to observe stars with existing spectroscopy, SDSS re-observed 245 of our stars as part of SEGUE (Yanny et al. 2009). We can use this independent data set to verify our velocity calibration. The mean difference between our heliocentric radial velocities and *elodiervfinal* from SDSS DR8 is 2 ± 27 km s^{-1}. The dispersion is consistent with the statistical uncertainties; 2 km s^{-1} is our systematic uncertainty.

Two epochs of spectroscopy also allow us to identify objects with variable radial velocity. Although no HVS exhibits a significant change in radial velocity, there are eight probable white dwarfs that exhibit $>4\sigma$ changes in velocity between the two epochs. We expect that these objects are compact binaries, and we are pursuing follow-up observations to confirm their velocity variability. To date, follow-up of low-mass $<0.25\,M_\odot$ white dwarfs in the HVS Survey has resulted in the discovery of two dozen merging, double-degenerate binaries with orbital periods as short as 12 minutes (Brown et al. 2010c, 2011a, 2011b, 2012; Kilic et al. 2010, 2011a, 2011b, 2011c, 2012).

2.3. Survey Completeness and Spectroscopic Identifications

With 1169 spectra in hand, the HVS Survey is now 90% complete for DR6- and DR7-selected candidates and 43% complete for DR8-selected candidates. The remaining candidates are concentrated at faint magnitudes $19.75 < g_0 < 20.25$ but are spread relatively evenly over the sky. This distribution of incompleteness is the result of many poor observing runs that prevented observations of the faintest objects in the survey.

Of the 1169 objects: 955 (82%) are normal stars with late-B spectral types, 192 (16%) are white dwarfs, 15 (1%) are quasars at $z \sim 2.4$, and 7 (1%) are B supergiant stars. The width and shape of the hydrogen Balmer lines provide a measure of surface gravity over our range of color (temperature). We use line indices described by Brown et al. (2003) to estimate spectral types, and we perform stellar atmosphere model fits for the late B-type objects using an upgraded version of the code described by Allende Prieto et al. (2006). The white dwarfs are studied in a series of papers on low-mass white dwarfs that begin with Kilic et al. (2007a, 2007b). The quasars were reported previously (Brown et al. 2009a). We discuss the B supergiants below, and focus the remainder of this paper on the 955 late B-type stars in the HVS Survey.

2.4. B Supergiants in the HVS Survey

Our spectra reveal seven B supergiants in the $\simeq 10,000$ deg^2 of sky sampled by our survey. All seven B supergiants are associated with known star-forming galaxies in the Local Group.

The first two B supergiants belong to the Leo A dwarf. We used those supergiants plus others to make the first stellar velocity dispersion measurement of Leo A (Brown et al. 2007a).

Four new B supergiants belong to M31 and trace its rotation curve. The stars are SDSS J003748.658+395402.57, SDSS J004108.023+401337.08, SDSS J004828.734+423158.58, and SDSS J004855.598+424629.99. The four stars have a mean apparent magnitude of $g_0 = 19.3$ and thus are located at the distance of M31 (Vilardell et al. 2010) for a typical B9 Ib luminosity of $M_g \simeq -5.0$. The stars have angular separations of $1°–2°$ from the center of M31 and locations consistent with the M31 disk. The two northern stars have systemic velocities of $+230$ km s^{-1} and $+250$ km s^{-1} with respect to M31, and the two southern stars have systemic velocities of -126 km s^{-1} and -200 km s^{-1} with respect to M31. The velocities perfectly match the H I rotation curve of M31 (Corbelli et al. 2010); the B supergiants clearly belong to the outer disk of M31.

The final B supergiant, SDSS J095951.180+052124.52, lies within $2.'5$ of the center of Sextans B. The star's 295 ± 4 km s^{-1} heliocentric radial velocity is identical with the velocity of Sextans B (Falco et al. 1999). Thus this B supergiant almost certainly belongs to Sextans B, and its existence is further evidence for on-going star formation in this Local Group dwarf. For a distance modulus of $(m-M)_0 = 25.56 \pm 0.10$ (Sakai et al. 1997) the $g_0 = 19.22$ star must have $M_g = -6.3$, consistent with a B9 Ia supergiant.

With absolute magnitudes of $M_g = -5$ to -6, the HVS Survey can detect B9 Ib/a supergiants to a depth of 1–2 Mpc. The only known star-forming galaxy undetected in our survey footprint is Pegasus, a dwarf that is known to have an extremely weak blue plume (Massey et al. 2007). M33 also falls in our footprint and was detected by our color selection, however we excluded M33 stars from the observing list because of obvious extended emission surrounding the stars. The absence of B supergiants elsewhere in the HVS Survey implies that there are no new star-forming galaxies in our survey footprint to a depth of 1–2 Mpc.

3. RESULTS

We now discuss the properties of our 955 late B-type stars and identify the unbound HVSs. For reference, Galactic escape velocity at the solar circle is 500–600 km s^{-1} (Smith et al. 2007) and at 50 kpc is 300–400 km s^{-1} (Gnedin et al. 2010).

3.1. Radial Velocity Distribution

Figure 2 plots the distribution of line-of-sight velocities corrected to the Galactic rest frame $v_{\rm rf}$ for the 955 late B-type stars in the HVS Survey. We calculate rest-frame velocities using the local standard of rest from Schönrich et al. (2010) and a 250 km s^{-1} circular rotation velocity (Reid et al. 2009; McMillan & Binney 2010):

$$v_{\rm rf} = v_{\rm helio} + 11.1\cos l\cos b + 262.24\sin l\cos b + 7.25\sin b. \quad (1)$$

This definition of $v_{\rm rf}$ changes our previous estimates of Galactic rest-frame velocity by up to 30 km s^{-1}. We note that $v_{\rm rf}$ represents the radial component of velocity in the Galactic rest frame, and is thus a lower limit to the true velocity of any HVS.

The 915 survey stars with $|v_{\rm rf}| < 275$ km s^{-1} have a 0 ± 4 km s^{-1} mean and a 107 ± 5 km s^{-1} dispersion, consistent with a stellar halo population. The velocity distribution, however, is not exactly Gaussian (Figure 2). King et al. (2012) show that 10%–17% of the HVS Survey stars may belong to the Sagittarius

---

[1] IRAF is distributed by the National Optical Astronomy Observatory, which is operated by the Association of Universities for Research in Astronomy, Inc., under cooperative agreement with the National Science Foundation.
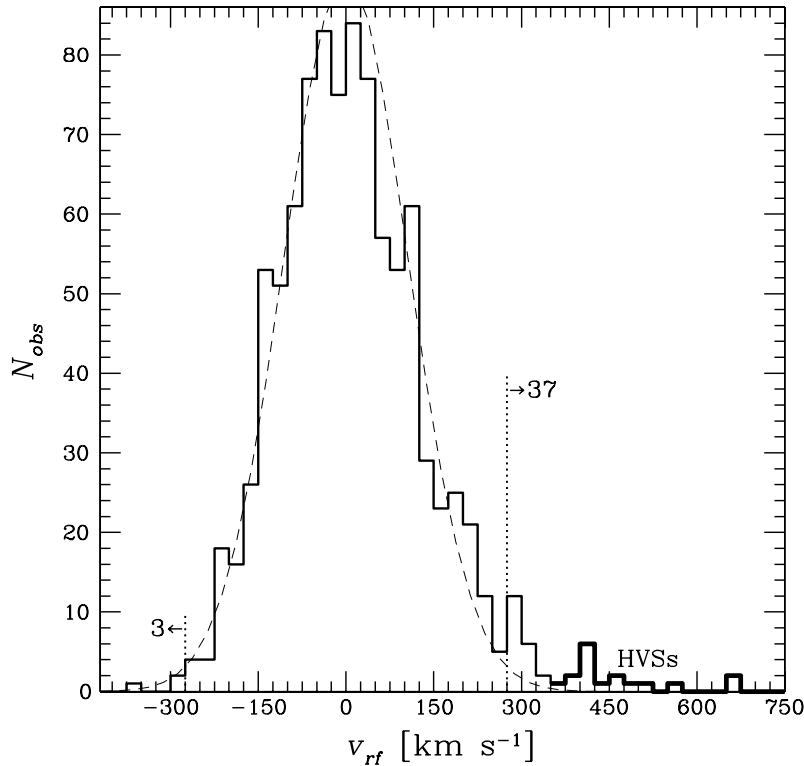
Figure 2. Minimum Galactic rest-frame velocity v_{rf} distribution for the 955 late B-type stars in the HVS Survey. The best-fit Gaussian (dashed line) has dispersion 107 km s^{-1}, excluding the 39 stars with $|v_{rf}| > 275$ km s^{-1}. The significant absence of $v_{rf} < -275$ km s^{-1} stars demonstrates that the positive velocity outliers are short-lived. Stars with $v_{rf} > 400$ km s^{-1} are unbound.

stream, which explains the excess of stars in the range -50 to -150 km s^{-1} and at $+100$ km s^{-1}.

Stars with $v_{rf} > +400$ km s^{-1} are unbound and probable HVSs. We observe no stars moving toward us with $v_{rf} < -400$ km s^{-1}, consistent with the picture that stars with $v_{rf} > +400$ km s^{-1} are ejected from the Milky Way. The most negative velocity star in our sample has $v_{rf} = -359 \pm 10$ km s^{-1}, consistent with Kenyon et al.'s (2008) estimate of escape velocity at 50 kpc. If the unbound stars are HVSs, then HVS ejection models show that we must also find a comparable number of bound HVSs in our survey (Bromley et al. 2006; Kenyon et al. 2008).

Indeed, we observe a significant excess of stars around $+300$ km s^{-1} that are possibly bound HVSs. As an estimate of significance, there is less than a 10^{-5} probability of randomly drawing 18 stars with 275 km s$^{-1} < v_{rf} < 325$ km s^{-1} from the tail of a Gaussian distribution with the observed parameters. Thus the excess of stars around $+300$ km s^{-1} are probably not halo stars. Because the stars around $+300$ km s^{-1} are bound to the Milky Way, the absence of a comparable number of stars at -300 km s^{-1} demonstrates that the bound stars must have main-sequence lifetimes less than their ~ 1 Gyr orbital turnaround times (Brown et al. 2007c; Kollmeier & Gould 2007; Yu & Madau 2007). We simply do not see stars falling back onto the Galaxy with similar velocities. Given the observed colors and spectra, we conclude that the stars around $+300$ km s^{-1} are main-sequence $\simeq 3\,M_\odot$ stars ejected into the outer halo.

3.2. Unbound Stars

We require distance estimates to determine whether a high velocity star is unbound. The observations demonstrate that high velocity stars are short-lived main-sequence stars. We

estimate luminosities by comparing observed colors to Girardi et al. (2002, 2004) stellar evolution tracks (see Figure 1) for solar abundance main-sequence stars. We use both $(u - g)_0$ and $(g - r)_0$ colors to estimate luminosity as described in Brown et al. (2010b). We estimate that the precision of our luminosities is ± 0.23 mag based on propagating color errors through the stellar evolution tracks with a Monte Carlo technique. We then calculate heliocentric distances using de-reddened apparent magnitudes, and convert to Galactocentric distances R assuming that the Sun is 8 kpc from the Galactic center.

Systematics are the dominant source of uncertainty in our distance estimates. The Girardi et al. (2002, 2004) absolute magnitudes are 0.24 ± 0.33 mag fainter than the Schaller et al. (1992) absolute magnitudes that we used in earlier HVS Survey papers. Thus our new luminosity estimates shift known HVSs to smaller distances. HVS7 suffers the biggest change, going from 60 kpc to 37 kpc; echelle spectroscopy, however, establishes that HVS7 is a 3.7 $M_\odot$ Bp star with $M_V \simeq -1.05$ (Przybilla et al. 2008c) and thus $\simeq 60$ kpc distant. This example highlights the uncertainty inherent in stellar evolution tracks. Stellar nature is another contributor to systematic uncertainty. We estimate a physical lower distance limit for our stars by assuming that they are evolved BHB stars. Dotter et al. (2007, 2008) tracks show that hot, metal-poor BHB stars are 1.33 ± 0.69 mag fainter than a main-sequence star of the same temperature in our survey. We indicate BHB distances with the horizontal error bars in Figure 3.

Figure 3 plots the resulting distribution of minimum Galactic rest-frame velocity v_{rf} versus Galactocentric distance R for the 37 stars with $v_{rf} > +275$ km s^{-1}. Identifying the unbound stars requires a potential model for the Galaxy. Because the Galactic potential is poorly constrained at large distances, we consider two recent models.
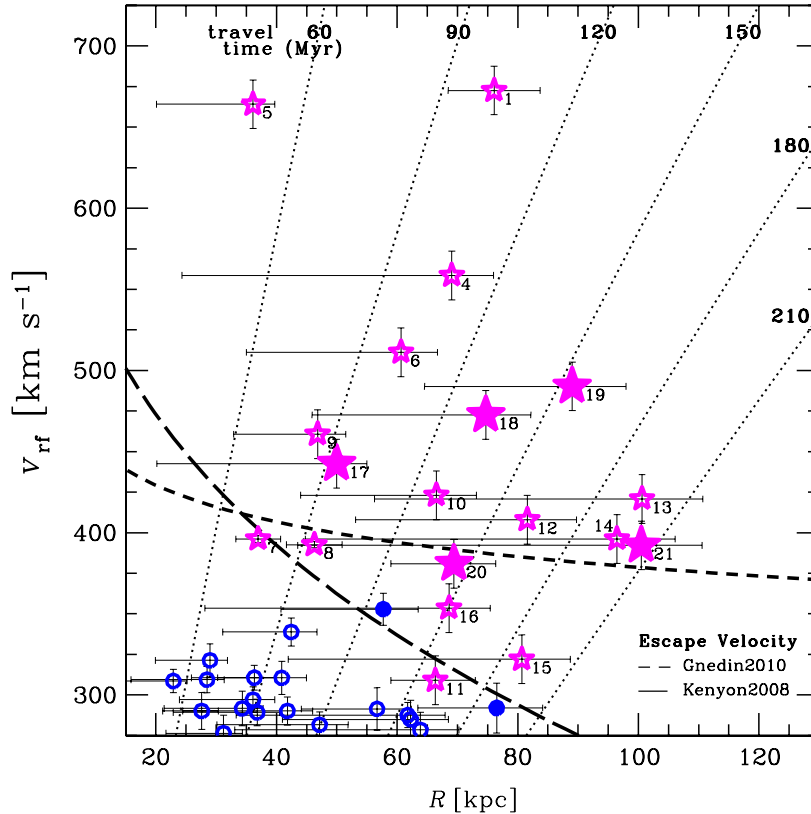
Figure 3. Minimum rest-frame velocity vs. Galactocentric distance R for all 37 stars with $v_{rf} > +275$ km s^{-1}. Distances are estimated using Girardi et al. (2004) main-sequence star tracks. Error bars show the span of physically possible distance given by evolved BHB tracks (Dotter et al. 2008). Five new HVSs (solid magenta stars) have velocities and distances exceeding the Gnedin et al. (2010) escape velocity model (dashed line). Other possible HVSs (solid blue dots) have velocities and distances near the Kenyon et al. (2008) escape velocity model (long dashed line). Previously identified HVSs are marked with open magenta stars. Isochrones of travel time from the Galactic center (dotted lines) are calculated assuming the observed minimum rest-frame velocity v_{rf} is the full space motion of the stars.

(A color version of this figure is available in the online journal.)

Kenyon et al. (2008) construct a spherically symmetric potential to fit observed Milky Way mass measurements from 5 pc to 10^5 pc. We estimate escape velocity from this model by dropping a test particle from rest at 250 kpc and calculating its infall velocity. This calculation yields an escape velocity of 360 km s^{-1} at 50 kpc (long-dashed line in Figure 3). Gnedin et al. (2010) measure the mass profile of the Milky Way using the velocity dispersion of the (bound) HVS Survey stars. Assuming that the escape velocity is twice the circular velocity, we estimate an escape velocity of 400 km s^{-1} at 50 kpc (dashed line in Figure 3). The escape velocity profiles differ in part because the Gnedin et al. (2010) dark matter halo is $1.6 \times 10^{12} M_{\odot}$ while the Kenyon et al. (2008) dark matter halo is $1 \times 10^{12} M_{\odot}$. The difference in escape velocity profiles illustrates the present uncertainties. Because a larger halo mass is preferred by recent observations (e.g., Przybilla et al. 2010), we use the Gnedin et al. (2010) model to identify new unbound stars.

We identify five new unbound HVSs with radial velocities and distances equaling or exceeding the Gnedin et al. (2010) escape velocity model, and one new possible HVS exceeding the Kenyon et al. (2008) escape velocity model. Previously we identified 14 unbound HVSs on the basis of the Kenyon et al. (2008) model, however our new v_{rf} and distance estimates place HVS11 slightly below the threshold of the Kenyon et al. (2008) model. Another two stars, HVS15 and HVS16, are above the threshold of the Kenyon et al. (2008) model but well below the threshold of the Gnedin et al. (2010) model. Therefore we re-classify these three objects as "possible HVSs." HVS7 and HVS8, on the other hand, are demonstrated $\simeq 4\,M_{\odot}$ main-

sequence B stars at $R \simeq 50$ kpc (López-Morales & Bonanos 2008; Przybilla et al. 2008c) and thus are almost certainly HVSs.

Table 1 summarizes the properties of all 37 HVS Survey stars with $v_{rf} > +275$ km s^{-1}. Columns include HVS number, heliocentric radial velocity $v_{\odot}$, minimum Galactic rest-frame velocity v_{rf} (not a full space velocity), de-reddened SDSS g-band magnitude, absolute magnitude M_g from Girardi et al. (2002, 2004) main-sequence tracks, Galactocentric distance R, Galactic coordinates (l, b), and catalog identification. There are 16 unbound HVSs, five possible HVSs, and 16 possibly bound HVSs.

The velocity and distance estimates allow us to estimate ejection times. The dotted lines in Figure 3 indicate travel times from the Galactic center under the assumption that v_{rf} is the three-dimensional velocity of our stars, a conservative assumption even though the orbits should be nearly radial (Gnedin et al. 2005). We find that HVSs are not clustered around a common ejection time, but have a range of ejection times spread continuously between 60 and 210 Myr. In other words, the observations do not support a large burst of HVSs that one might expect for binary MBH in-spiral or dwarf galaxy tidal disruption models. Rather, the observations support an ongoing ejection process, consistent with the Hills three-body ejection model.

4. FIVE NEW HYPERVELOCITY STARS

We discuss the details of the five new unbound HVSs discovered in this portion of the survey. All of the HVSs

Table 1
HVS Survey Stars with $v_{\rm rf} > +275$ km s^{-1}

ID	$v_\odot$ (km s^{-1})	$v_{\rm rf}$ (km s^{-1})	g_0 (mag)	M_g (mag)	$R_{\rm GC}$ (kpc)	l (deg)	b (deg)	Catalog	Reference
					HVSs				
HVS1	840	673	19.69	+0.41	76	227.33	+31.33	SDSS J090744.99+024506.88	1
HVS2	708	718	19.05	+2.6	26	175.99	+47.05	US708	2
HVS3	723	520	16.20	−2.7	62	263.04	−40.91	HE0437−5439	3
HVS4	611	559	18.31	−0.66	69	194.76	+42.56	SDSS J091301.01+305119.83	4
HVS5	553	664	17.56	+0.04	36	146.23	+38.70	SDSS J091759.47+672238.35	4
HVS6	626	511	18.97	+0.10	61	243.12	+59.56	SDSS J110557.45+093439.47	5
HVS7	529	396	17.64	−0.19	37	263.83	+57.95	SDSS J113312.12+010824.87	5
HVS8	489	393	17.94	+0.01	46	211.70	+46.33	SDSS J094214.03+200322.07	6
HVS9	628	461	18.64	+0.34	47	244.63	+44.38	SDSS J102137.08−005234.77	6
HVS10	478	423	19.22	+0.21	66	249.93	+75.72	SDSS J120337.85+180250.35	6
HVS12	552	408	19.61	+0.13	82	247.11	+52.46	SDSS J105009.59+031550.67	7
HVS13	575	421	20.02	+0.09	101	251.65	+50.64	SDSS J105248.30−000133.94	7
HVS14	532	396	19.72	−0.25	96	241.78	+53.20	SDSS J104401.75+061139.02	7
HVS17	246	442	17.43	−0.74	50	73.52	+41.16	SDSS J164156.39+472346.12	
HVS18	251	473	19.30	+0.05	75	103.64	−26.77	SDSS J232904.94+330011.47	
HVS19	597	490	20.06	+0.35	89	256.05	+63.74	SDSS J113517.75+080201.49	
HVS20	504	381	19.81	+0.54	69	262.56	+60.39	SDSS J113637.13+033106.84	
HVS21	355	392	19.73	−0.23	100	165.26	+56.11	SDSS J103418.25+481134.57	
					Possible HVSs				
HVS11	477	307	19.58	+0.68	64	238.77	+40.63	SDSS J095906.47+000853.41	7
	222	292	19.83	+0.53	77	155.50	+49.46	SDSS J101359.79+563111.65	7
	496	353	18.86	+0.28	54	256.27	+54.55	SDSS J111136.44+005856.44	
HVS15	463	322	19.15	−0.29	78	266.51	+55.92	SDSS J113341.09−012114.25	7
HVS16	434	345	19.33	−0.03	74	285.86	+67.38	SDSS J122523.40+052233.84	7
					Possible Bound HVSs				
	150	321	17.14	+0.29	27	115.82	−40.58	SDSS J002810.33+215809.66	
	136	311	17.77	+0.03	40	125.05	−31.26	SDSS J005956.06+313439.29	
	108	276	17.19	+0.18	30	127.53	−31.42	SDSS J010948.30+311727.66	
	361	288	18.39	−0.25	61	196.07	+23.21	SDSS J074950.24+243841.16	7
	229	297	17.28	+0.06	34	160.45	+34.20	SDSS J081828.07+570922.07	7
	306	282	18.08	+0.14	45	186.30	+42.16	SDSS J090710.07+365957.54	7
	504	339	18.48	+0.39	44	247.97	+46.42	SDSS J103357.26−011507.35	
	448	285	19.23	+0.14	68	250.71	+47.87	SDSS J104318.29−013502.51	
	482	309	17.38	+0.08	30	269.75	+47.30	SDSS J112255.77−094734.92	
	140	291	19.13	+0.47	58	130.08	+40.59	SDSS J112359.47+751807.73	
	424	290	18.13	−0.07	44	274.88	+57.45	SDSS J115245.91−021116.21	7
	228	309	17.49	+0.06	31	65.34	+72.37	SDSS J140432.38+352258.41	7
	284	289	18.40	+0.22	40	357.16	+63.62	SDSS J141723.34+101245.74	7
	206	278	18.88	−0.12	58	18.68	+44.85	SDSS J154806.92+093423.93	
	62	292	17.51	+0.12	29	75.71	+28.06	SDSS J180050.86+482424.63	
	133	290	17.35	+0.41	25	85.47	−51.67	SDSS J232229.47+043651.45	

References. (1) Brown et al. 2005; (2) Hirsch et al. 2005; (3) Edelmann et al. 2005; (4) Brown et al. 2006a; (5) Brown et al. 2006b; (6) Brown et al. 2007c; (7) Brown et al. 2009a.

except for HVS17 have multiple epochs of observation. None of the HVSs exhibit significant radial velocity variations, which indicates that the HVSs are unlikely to be compact binaries.

SDSS J164156.391+472346.12, hereafter HVS17, has a $+246 \pm 9$ km s^{-1} heliocentric radial velocity and a minimum velocity of $v_{\rm rf} = +443$ in the Galactic frame. HVS17 is the hottest HVS in our survey with a B6 spectral type. HVS17 is also the brightest HVS in our survey, $g = 17.499 \pm 0.015$ mag, opening the possibility of follow-up echelle spectroscopy. A solar metallicity $4\,M_\odot$ star with the temperature of HVS17 has $M_g = -0.74$ (Girardi et al. 2002, 2004) and a distance of $R = 50$ kpc.

SDSS J232904.947+330011.47, hereafter HVS18, has a $+251 \pm 10$ km s^{-1} heliocentric radial velocity and a minimum velocity of $v_{\rm rf} = +473$ in the Galactic frame. At

$b = -26.8°$, HVS18 is the lowest latitude HVS in our survey. HVS18 is also our first HVS discovery in the southern Galactic hemisphere. Unlike HVS3, the $9\,M_\odot$ HVS near the LMC (Edelmann et al. 2005; Przybilla et al. 2008b), HVS18 is 17° from M31. Any association with M31 or its satellites is impossible. A solar metallicity $3\,M_\odot$ star with the temperature of HVS18 has $M_g = 0.05$, thus HVS18 has a distance of $R = 75$ kpc from the Milky Way and a distance of 700 kpc from M31.

SDSS J113517.759+080201.49, hereafter HVS19, has a $+597 \pm 15$ km s^{-1} heliocentric radial velocity and a minimum velocity of $v_{\rm rf} = +490$ in the Galactic frame. HVS19 is one of the cooler HVSs in our survey with an A0 spectral type. A solar metallicity $\simeq 2.5\,M_\odot$ star with the temperature of HVS19 has $M_g = 0.35$, which puts its location at $R = 90$ kpc. Like many of the other HVSs, HVS19 is in the constellation of Leo.
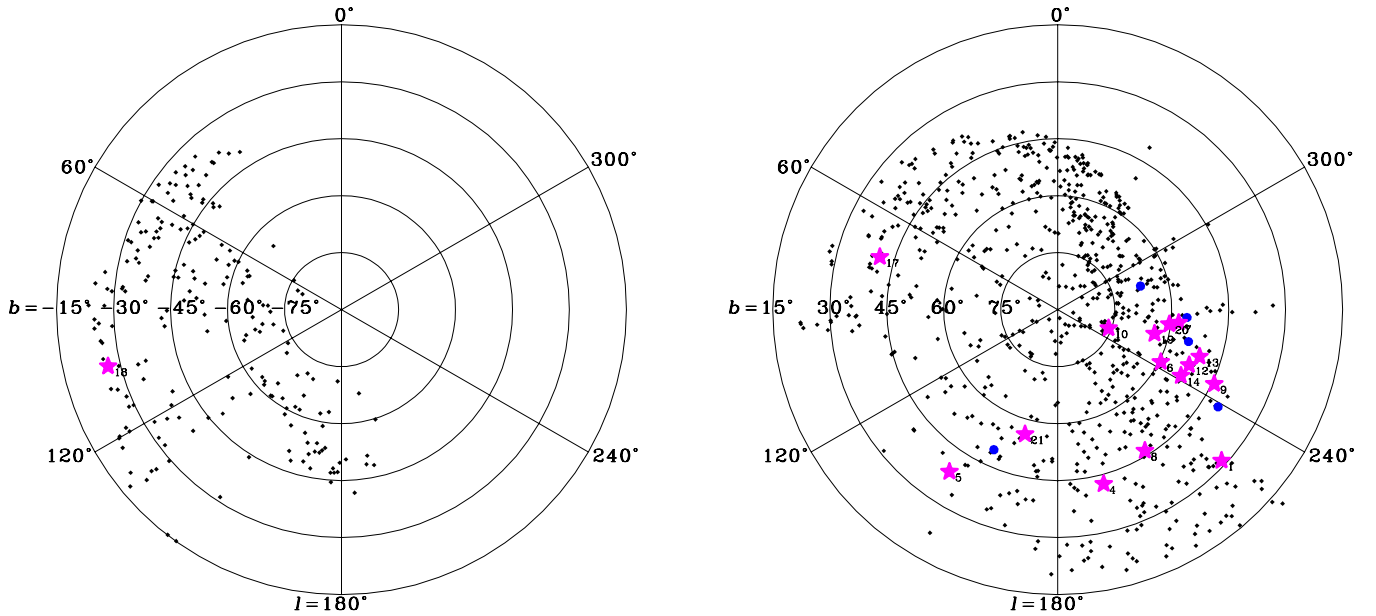
Figure 4. Polar projections, in Galactic coordinates, showing the 16 unbound HVSs (magenta stars), the five possible HVSs (blue circles), and the 934 other stars (black dots) in the HVS Survey over the southern (left) and northern (right) Galactic caps.

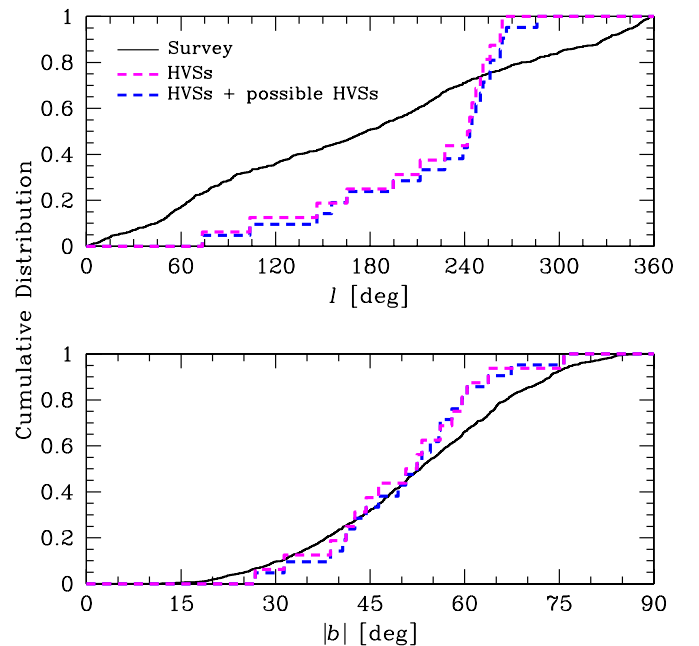(A color version of this figure is available in the online journal.)

SDSS J113637.135+033106.84, hereafter HVS20, has a 504 ± 12 km s^{-1} heliocentric radial velocity and a minimum velocity of $v_{\rm rf} = +381$ km s^{-1} in the Galactic frame. HVS20 sits on the escape velocity threshold of Gnedin et al. (2010) but is well above the threshold of Kenyon et al. (2008). HVS20 is similar to HVS19, only 4°.5 away; it is yet another HVS in the constellation Leo. HVS20 is also one of the coolest HVSs in our survey with an A1 spectral type. With an estimated luminosity of $M_g = 0.54$, HVS20 sits at $R = 80$ kpc and so shares a similar ejection time as HVS19. The other eight HVSs around Leo have ejection times that differ by up to 125 Myr, however, implying that the HVSs in the direction of Leo do not all come from a single ejection event.

SDSS J103418.254+481134.57, hereafter HVS21, has a $+355 \pm 10$ km s^{-1} heliocentric radial velocity and a minimum velocity of $v_{\rm rf} = +392$ km s^{-1} in the Galactic frame. HVS21 has a B7 spectral type and, for a luminosity of $M_g = -0.23$, is located at $R = 100$ kpc. Like HVS20, HVS21 sits on escape velocity threshold of Gnedin et al. (2010) but is well above the threshold of Kenyon et al. (2008). HVS21 is in Ursa Major about 11° from HVS2 (Hirsch et al. 2005).

5. SPATIAL ANISOTROPY

The spatial distribution of HVSs on the sky is intriguing because it is almost certainly linked to their origin. In principle, the MBH in the Galactic center can eject HVSs in all directions. Brown et al. (2009b) demonstrate that unbound HVSs have a significantly anisotropic distribution on the sky. Lower velocity bound HVSs have a more isotropic distribution. The new HVSs reported here support these trends.

Figure 4 plots the angular positions of all of the survey stars. The overall distribution of positions reflects the SDSS imaging footprint. HVSs are marked with solid magenta stars and possible HVSs are marked with solid blue dots. The stars have a similar distribution and so we consider the combined set of HVSs in an attempt to mitigate small number statistics. Because of the complex SDSS footprint and because of the

Figure 5. Cumulative distributions of Galactic l and b of the 16 unbound HVSs (dashed magenta line), 21 HVSs and possible HVSs (dashed blue line), and the other stars (solid line) in the HVS Survey.

(A color version of this figure is available in the online journal.)

HVS Survey incompleteness, we quantify the spatial anisotropy by comparing the distribution of HVSs against the distribution of observed stars from which they are drawn. Although this comparison is not perfect—the overdensity of stars arcing to the right of the North Galactic pole in Figure 4 is the Sgr stream—this approach provides a fair comparison of positions and angular separations in the HVS Survey.

Figure 5 plots the cumulative Galactic longitude and latitude distributions of our survey stars and HVSs. Kolmogorov–Smirnov (K-S) tests find 0.013 and 0.415 likelihoods that the combined set of HVSs are drawn from the same

longitude and latitude distributions, respectively, as the survey stars. The longitude and latitude tests are not completely independent because of the complex boundaries of our survey region. The K-S tests establish, however, that the HVS spatial anisotropy is primarily in Galactic longitude and not in Galactic latitude.

Next we consider the distribution of angular separations. Seven of the HVSs (33%) are in the constellation Leo, thus we expect that the HVSs have an excess of small angular separations and an absence of large angular separations compared with the survey stars. Calculating the angular separations for all unique pairs of stars, a K-S test finds a 3×10^{-18} likelihood that the HVSs are drawn from the same distribution of angular separations as the survey stars. We establish the significance of this likelihood by taking 10,000 random draws of 21 unique stars from the survey: a likelihood below 3×10^{-18} occurs at random 0.3% of the time in our survey. The actual significance of the anisotropy depends on the method of calculation; our approach indicates a formal significance of 3σ.

A number of models propose to explain the HVS spatial anisotropy. Abadi et al. (2009) propose a tidal debris origin for HVSs (see also Piffl et al. 2011). However, this model is difficult to reconcile with the observations because (1) known HVSs have ejection times that differ by up to 150 Myr, (2) no other unbound tidal debris is observed in the same region of sky (Kollmeier et al. 2009, 2010), and (3) no dwarf galaxy in the Local Group has comparable velocity. An intermediate-mass black hole in-spiral event in the Galactic center may produce a ring of HVSs around the sky (Gualandris et al. 2005; Levin 2006; Sesana et al. 2006; Baumgardt et al. 2006) but this model is also at variance with the observations. Theoretically predicted black hole in-spirals occur on timescales 10–100 times shorter than the observed span of HVS ejection times, thus multiple black hole in-spiral events with common alignment are necessary to account for the observed spatial distribution.

Runaway stars, stars born in the disk and ejected by binary disruptions, are another possible source of apparent HVSs (e.g., Gvaramadze et al. 2009). Surveys of stars near the Galactic disk identify unbound stars ejected from the disk (Heber et al. 2008; Przybilla et al. 2008a; Tillich et al. 2009; Irrgang et al. 2010) as expected in runaway star mechanisms (Bromley et al. 2009; Gvaramadze 2009). Stars ejected from a rotating disk have a distinct spatial distribution: The fastest stars are those ejected in the direction of Galactic rotation, thus ≃90% of >400 km s^{-1} runaways should be located $|b| < 45°$ (Bromley et al. 2009). Moreover, >400 km s^{-1} runaways at $R = 50$ kpc should be found over all Galactic longitudes. Thus the expected distribution of runaway latitudes and longitudes is inconsistent with the observed distribution of HVSs.

The ejection *rate* of disk runaways is also inconsistent with the observed number of HVSs. The physical size of stars places a speed limit on stellar binary disruption mechanisms: A 3 $M_\odot$ runaway with $v_{rf} > +400$ km s^{-1} at $R = 50$ kpc requires the disruption of a compact binary containing a massive star within its lifetime while avoiding a merger. An optimistic ejection rate for 3 $M_\odot$ runaways with >400 km s^{-1} at $R = 50$ kpc is about 100–100,000 times smaller than the expected rate of HVSs ejected by the MBH (Brown et al. 2009a; Perets & Subr 2012). Given that the HVSs are not clustered at low latitudes in our survey, we conclude that runaways are unlikely contaminants to the HVS sample.

The anisotropic distribution of stars in the Galactic center provides another model for explaining the anisotropy of HVSs.

If the central MBH is the origin of HVSs, and the stars orbiting near the MBH are concentrated in one or two disks (Levin & Beloborodov 2003; Lu et al. 2009; Bartko et al. 2009), then stars probably interact with the MBH in preferred planes. Lu et al. (2010) and Zhang et al. (2010) demonstrate that the observed distribution of HVSs is consistent with two thin disk planes aligned with the present stellar disks in the Galactic center. Observed HVSs were ejected up to 200 Myr ago, however. Although the Galactic center clearly contains anisotropic structure—including young stellar clusters like the Arches and Quintuplet clusters and gaseous disks, arms, and bars that may form young stars—there is no model that explains how Galactic center structure maintains a fixed orientation for 200 Myr.

A final model is an anisotropic Galactic potential. HVSs are unique test particles because they start in the Galactic center and travel to infinity. The gravitational potential maps initial HVS ejection velocities to the velocities that we observe in the outer halo today. Because many HVSs are marginally unbound, a non-spherical potential can naturally explain why HVSs are found in preferred directions on the sky: Stars ejected along the long axis of the potential would have the fastest observed velocities; stars ejected along the minor axis of the potential are decelerated more and therefore, fewer will be observed as HVSs. Kenyon et al. (2008) show that the important quantity is the scale length of potential in the central 10–100 pc, the region where HVSs experience the most deceleration. The anisotropic potential model can be tested with the all-sky distribution of HVSs. If there is rotation around the long axis of the potential, stars ejected along the long axis should be located in two clumps on opposite points in the sky. If there is rotation around the short axis, stars ejected along the long axis should appear in ring of HVSs around the sky. There are currently no good constraints on the shape and orientation of the Galactic potential, but perhaps the HVSs will reveal it.

6. CONCLUSIONS

We report new results from our targeted HVS Survey, a spectroscopic survey of stars with ≃3 $M_\odot$ colors that should not exist at faint magnitudes unless they were ejected into the outer halo as HVSs. Our survey is 90% complete for SDSS DR6- and DR7-selected candidates and 43% complete for DR8-selected candidates. Spectroscopy reveals that most of the candidates are normal late B-type stars in the halo; other objects include low-mass white dwarf binaries and B supergiants in known star-forming galaxies. The absence of B supergiants elsewhere in the HVS Survey implies that there are no new star-forming galaxies to a depth of 1–2 Mpc within our survey footprint.

The velocity distribution of the 955 late B-type stars in the survey is remarkable: 37 stars have $v_{rf} > +275$ km s^{-1} and three stars have $v_{rf} < -275$ km s^{-1}. The observational signature of an HVS is its unbound velocity, which we determine by comparing observed radial velocities and distances to Galactic potential models. There are five new unbound HVSs on the basis of the Gnedin et al. (2010) escape velocity model. The HVS Survey thus identifies 16 unbound HVSs, five possible HVSs, and 16 possibly bound HVSs.

A Galactic center origin for the HVSs is supported by their unbound velocities, the observed number of unbound stars, their stellar nature, their ejection time distribution, and their Galactic latitude and longitude distribution. Other proposed origins for the unbound HVSs, including runaway ejections from the disk

Table 2
Late B-type Halo Stars in the HVS Survey

R.A. (hr)	Decl. (deg)	g (mag)	$v_\odot$ (km s^{-1})	v_{rf} (km s^{-1})	l (deg)	b (deg)
0:01:31.115	+26:46:55.06	19.671 ± 0.021	−374.4 ± 11.8	−178.3	109.35	−34.77
0:02:33.817	−09:57:06.85	18.578 ± 0.021	−87.7 ± 7.7	−1.8	86.76	−69.32
0:05:28.141	−11:00:10.07	19.271 ± 0.042	−115.9 ± 9.2	−35.5	86.89	−70.59
0:05:51.194	+32:56:35.75	18.075 ± 0.020	−250.5 ± 8.7	−44.9	112.01	−28.96
0:07:00.445	−19:46:13.52	18.304 ± 0.029	8.9 ± 9.7	55.0	66.44	−77.44
0:07:57.158	−06:02:46.37	18.123 ± 0.017	−124.7 ± 12.4	−27.6	94.85	−66.52
0:12:26.890	−10:47:54.56	19.042 ± 0.025	−128.2 ± 8.7	−51.0	91.74	−71.27
0:13:00.653	−20:23:31.26	18.511 ± 0.071	−40.4 ± 11.3	0.1	68.37	−78.93
0:15:58.669	+33:48:40.41	17.494 ± 0.018	8.2 ± 11.0	210.3	114.56	−28.48
0:17:22.694	+32:33:54.26	19.592 ± 0.019	46.9 ± 11.3	246.1	114.67	−29.76

(This table is available in its entirety in a machine-readable form in the online journal. A portion is shown here for guidance regarding its form and content.)

or dwarf galaxy tidal debris, cannot easily be reconciled with the observations. Although not all unbound stars are necessarily HVSs, the MBH ejection origin provides the best explanation for the observed $\simeq 3\,M_\odot$ unbound HVSs in our survey.

HVSs are important because their properties are tied to the nature and environment of the MBH that ejects them (Portegies Zwart et al. 2006; Merritt 2006; Demarque & Virani 2007; Ginsburg & Loeb 2007; Gualandris & Portegies Zwart 2007; Hansen 2007; Lu et al. 2007; Sesana et al. 2007a, 2007b, 2008, 2009; O'Leary & Loeb 2008; Perets & Alexander 2008; Perets 2009a, 2009b; Sherwin et al. 2008; Svensson et al. 2008; Löckmann & Baumgardt 2008; Löckmann et al. 2008, 2009; Chen et al. 2009; Gualandris & Merritt 2009; Hopman 2009; Madigan et al. 2009; Sari et al. 2010; Antonini et al. 2010, 2011; Baruteau et al. 2011; Ginsburg & Perets 2012). HVSs are also important probes of the dark matter potential through which they move (Gnedin et al. 2005; Yu & Madau 2007; Wu et al. 2008; Kenyon et al. 2008; Perets et al. 2009b).

An intriguing result of the HVS Survey is the spatial anisotropy of unbound HVSs on the sky. There is as yet no compelling explanation for the anisotropy. We speculate that an anisotropic central potential may explain the observations. In the future, measuring the full space trajectories of the HVSs promises to elucidate the origin of HVSs (Brown et al. 2010a) and better constrain the shape and orientation of the Galactic potential. Further progress requires measuring the spatial distribution of HVSs over the entire sky. We look forward to using the Skymapper Survey (Keller et al. 2007) to identify HVS candidates in coming years.

Facility: MMT (Blue Channel Spectrograph)

APPENDIX

DATA TABLE

Table 2 presents the sample of 955 late B-type stars in the HVS Survey studied here. For completeness, we provide both the 375 newly observed objects and the 580 previously reported objects. Columns include J2000 coordinates, SDSS *g*-band apparent magnitude, our heliocentric velocity, velocity in the Galactic rest-frame (Equation (1)), and Galactic longitude and latitude.

REFERENCES

Abadi, M. G., Navarro, J. F., & Steinmetz, M. 2009, ApJ, 691, L63
Aihara, H., Allende Prieto, C., An, D., et al. 2011, ApJS, 193, 29
Allende Prieto, C., Beers, T. C., Wilhelm, R., et al. 2006, ApJ, 636, 804
Antonini, F., Faber, J., Gualandris, A., & Merritt, D. 2010, ApJ, 713, 90
Antonini, F., Lombardi, J. C., Jr., & Merritt, D. 2011, ApJ, 731, 128
Bartko, H., Martins, F., Fritz, T. K., et al. 2009, ApJ, 697, 1741
Baruteau, C., Cuadra, J., & Lin, D. N. C. 2011, ApJ, 726, 28
Baumgardt, H., Gualandris, A., & Portegies Zwart, S. 2006, MNRAS, 372, 174
Blaauw, A. 1961, Bull. Astron. Inst. Neth., 15, 265
Bromley, B. C., Brown, W. R., Geller, M. J., & Kenyon, S. J. 2009, ApJ, 706, 925
Bromley, B. C., Kenyon, S. J., Geller, M. J., & Brown, W. R. 2012, ApJ, 749, L42
Bromley, B. C., Kenyon, S. J., Geller, M. J., et al. 2006, ApJ, 653, 1194
Brown, W. R., Allende Prieto, C., Beers, T. C., et al. 2003, AJ, 126, 1362
Brown, W. R., Anderson, J., Gnedin, O. Y., et al. 2010a, ApJ, 719, L23
Brown, W. R., Geller, M. J., & Kenyon, S. J. 2009a, ApJ, 690, 1639
Brown, W. R., Geller, M. J., Kenyon, S. J., & Bromley, B. C. 2009b, ApJ, 690, L69
Brown, W. R., Geller, M. J., Kenyon, S. J., & Diaferio, A. 2010b, AJ, 139, 59
Brown, W. R., Geller, M. J., Kenyon, S. J., & Kurtz, M. J. 2005, ApJ, 622, L33
Brown, W. R., Geller, M. J., Kenyon, S. J., & Kurtz, M. J. 2006a, ApJ, 640, L35
Brown, W. R., Geller, M. J., Kenyon, S. J., & Kurtz, M. J. 2006b, ApJ, 647, 303
Brown, W. R., Geller, M. J., Kenyon, S. J., & Kurtz, M. J. 2007a, ApJ, 666, 231
Brown, W. R., Geller, M. J., Kenyon, S. J., Kurtz, M. J., & Bromley, B. C. 2007b, ApJ, 660, 311
Brown, W. R., Geller, M. J., Kenyon, S. J., Kurtz, M. J., & Bromley, B. C. 2007c, ApJ, 671, 1708
Brown, W. R., Kilic, M., Allende Prieto, C., & Kenyon, S. J. 2010c, ApJ, 723, 1072
Brown, W. R., Kilic, M., Allende Prieto, C., & Kenyon, S. J. 2011a, MNRAS, 411, L31
Brown, W. R., Kilic, M., Allende Prieto, C., & Kenyon, S. J. 2012, ApJ, 744, 142
Brown, W. R., Kilic, M., Hermes, J. J., et al. 2011b, ApJ, 737, L23
Chen, X., Madau, P., Sesana, A., & Liu, F. K. 2009, ApJ, 697, L149
Corbelli, E., Lorenzoni, S., Walterbos, R., Braun, R., & Thilker, D. 2010, A&A, 511, A89
Davies, M. B., King, A., & Ritter, H. 2002, MNRAS, 333, 463
Demarque, P., & Virani, S. 2007, A&A, 461, 651
Dotter, A., Chaboyer, B., Jevremović, D., et al. 2007, AJ, 134, 376
Dotter, A., Chaboyer, B., Jevremović, D., et al. 2008, ApJS, 178, 89
Edelmann, H., Napiwotzki, R., Heber, U., Christlieb, N., & Reimers, D. 2005, ApJ, 634, L181
Falco, E. E., Kurtz, M. J., Geller, M. J., et al. 1999, PASP, 111, 438
Fuentes, C. I., Stanek, K. Z., Gaudi, B. S., et al. 2006, ApJ, 636, L37
Ghez, A. M., Salim, S., Hornstein, S. D., et al. 2005, ApJ, 620, 744
Ghez, A. M., Salim, S., Weinberg, N. N., et al. 2008, ApJ, 689, 1044

Gillessen, S., Eisenhauer, F., Fritz, T. K., et al. 2009a, ApJ, 707, L114
Gillessen, S., Eisenhauer, F., Trippe, S., et al. 2009b, ApJ, 692, 1075
Ginsburg, I., & Loeb, A. 2006, MNRAS, 368, 221
Ginsburg, I., & Loeb, A. 2007, MNRAS, 376, 492
Ginsburg, I., & Perets, H. B. 2012, MNRAS, submitted (arXiv:1109.2284)
Girardi, L., Bertelli, G., Bressan, A., et al. 2002, A&A, 391, 195
Girardi, L., Grebel, E. K., Odenkirchen, M., & Chiosi, C. 2004, A&A, 422, 205
Gnedin, O. Y., Brown, W. R., Geller, M. J., & Kenyon, S. J. 2010, ApJ, 720, L108
Gnedin, O. Y., Gould, A., Miralda-Escudé, J., & Zentner, A. R. 2005, ApJ, 634, 344
Gualandris, A., & Merritt, D. 2009, ApJ, 705, 361
Gualandris, A., & Portegies Zwart, S. 2007, MNRAS, 376, L29
Gualandris, A., Portegies Zwart, S. P., & Sipior, M. S. 2005, MNRAS, 363, 223
Gvaramadze, V. V. 2009, MNRAS, 395, L85
Gvaramadze, V. V., Gualandris, A., & Portegies Zwart, S. 2009, MNRAS, 396, 570
Hansen, B. M. S. 2007, ApJ, 671, L133
Heber, U., Edelmann, H., Napiwotzki, R., Altmann, M., & Scholz, R.-D. 2008, A&A, 483, L21
Hills, J. G. 1988, Nature, 331, 687
Hirsch, H. A., Heber, U., O'Toole, S. J., & Bresolin, F. 2005, A&A, 444, L61
Hopman, C. 2009, ApJ, 700, 1933
Irrgang, A., Przybilla, N., Heber, U., Fernanda Nieva, M., & Schuh, S. 2010, ApJ, 711, 138
Keller, S. C., Schmidt, B. P., Bessell, M. S., et al. 2007, PASA, 24, 1
Kenyon, S. J., Bromley, B. C., Geller, M. J., & Brown, W. R. 2008, ApJ, 680, 312
Kilic, M., Allende Prieto, C., Brown, W. R., & Koester, D. 2007a, ApJ, 660, 1451
Kilic, M., Brown, W. R., Allende Prieto, C., Kenyon, S. J., & Panei, J. A. 2010, ApJ, 716, 122
Kilic, M., Brown, W. R., Allende Prieto, C., Pinsonneault, M., & Kenyon, S. 2007b, ApJ, 664, 1088
Kilic, M., Brown, W. R., Allende Prieto, C., et al. 2011a, ApJ, 727, 3
Kilic, M., Brown, W. R., Hermes, J. J., et al. 2011b, MNRAS, 418, L157
Kilic, M., Brown, W. R., Kenyon, S. J., et al. 2011c, MNRAS, 413, L101
Kilic, M., Brown, W. R., Allende Prieto, C., et al. 2012, ApJ, in press (arXiv:1204.0028)
King, C., III, Brown, W. R., Geller, M. J., & Kenyon, S. J. 2012, ApJ, in press (arXiv:1112.1919)
Kollmeier, J. A., & Gould, A. 2007, ApJ, 664, 343
Kollmeier, J. A., Gould, A., Knapp, G., & Beers, T. C. 2009, ApJ, 697, 1543
Kollmeier, J. A., Gould, A., Rockosi, C., et al. 2010, ApJ, 723, 812
Kurtz, M. J., & Mink, D. J. 1998, PASP, 110, 934
Leonard, P. J. T. 1991, AJ, 101, 562
Leonard, P. J. T. 1993, in ASP Conf. Ser. 45, Luminous High-Latitude Stars, ed. D. Sasselov (San Francisco, CA: ASP), 360
Leonard, P. J. T., & Duncan, M. J. 1988, AJ, 96, 222
Leonard, P. J. T., & Duncan, M. J. 1990, AJ, 99, 608
Levin, Y. 2006, ApJ, 653, 1203
Levin, Y., & Beloborodov, A. M. 2003, ApJ, 590, L33
Löckmann, U., & Baumgardt, H. 2008, MNRAS, 384, 323

Löckmann, U., Baumgardt, H., & Kroupa, P. 2008, ApJ, 683, L151
Löckmann, U., Baumgardt, H., & Kroupa, P. 2009, MNRAS, 398, 429
López-Morales, M., & Bonanos, A. Z. 2008, ApJ, 685, L47
Lu, J. R., Ghez, A. M., Hornstein, S. D., et al. 2009, ApJ, 690, 1463
Lu, Y., Yu, Q., & Lin, D. N. C. 2007, ApJ, 666, L89
Lu, Y., Zhang, F., & Yu, Q. 2010, ApJ, 709, 1356
Madigan, A.-M., Hopman, C., & Levin, Y. 2011, ApJ, 738, 99
Madigan, A.-M., Levin, Y., & Hopman, C. 2009, ApJ, 697, L44
Massey, P., Olsen, K. A. G., Hodge, P. W., et al. 2007, AJ, 133, 2393
McMillan, P. J., & Binney, J. J. 2010, MNRAS, 402, 934
Merritt, D. 2006, ApJ, 648, 976
O'Leary, R. M., & Loeb, A. 2008, MNRAS, 383, 86
O'Leary, R. M., & Loeb, A. 2009a, ApJ, 690, 795
O'Leary, R. M., & Loeb, A. 2009b, ApJ, 698, 1330
Perets, H. B., & Alexander, T. 2008, ApJ, 677, 146
Perets, H. B., Gualandris, A., Merritt, D., & Alexander, T. 2009a, ApJ, 702, 884
Perets, H. B., Hopman, C., & Alexander, T. 2007, ApJ, 656, 709
Perets, H. B., & Subr, L. 2012, ApJ, submitted (arXiv:1202.2356)
Perets, H. B., Wu, X., Zhao, H. S., et al. 2009b, ApJ, 697, 2096
Piffl, T., Williams, M., & Steinmetz, M. 2011, A&A, 535, A70
Portegies Zwart, S. F. 2000, ApJ, 544, 437
Portegies Zwart, S. F., Baumgardt, H., McMillan, S. L. W., et al. 2006, ApJ, 641, 319
Poveda, A., Ruiz, J., & Allen, C. 1967, Bol. Obs. Tonantzintla Tacubaya, 4, 860
Przybilla, N., Nieva, M. F., Heber, U., & Butler, K. 2008a, ApJ, 684, L103
Przybilla, N., Nieva, M. F., Heber, U., et al. 2008b, A&A, 480, L37
Przybilla, N., Nieva, M. F., Tillich, A., et al. 2008c, A&A, 488, L51
Przybilla, N., Tillich, A., Heber, U., & Scholz, R.-D. 2010, ApJ, 718, 37
Reid, M. J., Menten, K. M., Zheng, X. W., et al. 2009, ApJ, 700, 137
Sakai, S., Madore, B. F., & Freedman, W. L. 1997, ApJ, 480, 589
Sari, R., Kobayashi, S., & Rossi, E. M. 2010, ApJ, 708, 605
Schaller, G., Schaerer, D., Meynet, G., & Maeder, A. 1992, A&AS, 96, 269
Schmidt, G. D., Weymann, R. J., & Foltz, C. B. 1989, PASP, 101, 713
Schönrich, R., Binney, J., & Dehnen, W. 2010, MNRAS, 403, 1829
Sesana, A., Haardt, F., & Madau, P. 2006, ApJ, 651, 392
Sesana, A., Haardt, F., & Madau, P. 2007a, ApJ, 660, 546
Sesana, A., Haardt, F., & Madau, P. 2007b, MNRAS, 379, L45
Sesana, A., Haardt, F., & Madau, P. 2008, ApJ, 686, 432
Sesana, A., Madau, P., & Haardt, F. 2009, MNRAS, 392, L31
Sherwin, B. D., Loeb, A., & O'Leary, R. M. 2008, MNRAS, 386, 1179
Smith, M. C., Ruchti, G. R., Helmi, A., et al. 2007, MNRAS, 379, 755
Svensson, K. M., Church, R. P., & Davies, M. B. 2008, MNRAS, 383, L15
Tauris, T. M., & Takens, R. J. 1998, A&A, 330, 1047
Tillich, A., Przybilla, N., Scholz, R., & Heber, U. 2009, A&A, 507, L37
Vilardell, F., Ribas, I., Jordi, C., Fitzpatrick, E. L., & Guinan, E. F. 2010, A&A, 509, A70
Wu, X., Famaey, B., Gentile, G., Perets, H., & Zhao, H. 2008, MNRAS, 386, 2199
Yanny, B., Rockosi, C., Newberg, H. J., et al. 2009, AJ, 137, 4377
Yu, Q., & Madau, P. 2007, MNRAS, 379, 1293
Yu, Q., & Tremaine, S. 2003, ApJ, 599, 1129
Zhang, F., Lu, Y., & Yu, Q. 2010, ApJ, 722, 1744